DOI:
10.1109/TBME.2019.2909994

Document Version
Peer reviewed version

Real-time Passive Brain Monitoring System Using Near-Field Microwave Radiometry

Evangelos Groumpas, Maria Koutsoupidou, Irene S. Karanasiou, Charalabos Papageorgiou and Nikolaos Uzunoglu, *Fellow, IEEE*

Abstract— *Objective*: Near-field microwave radiometry has emerged as a tool for real time passive monitoring of local brain activation possibly attributed to local changes in blood flow that correspond to temperature and/or conductivity changes. The aim of this study is to design and evaluate a prototype system based on microwave radiometry intended to detect local changes of temperature and conductivity in depth in brain tissues. A novel radiometric system that comprises a four port total power Dicke-switch sensitive receiver that operates at 1.5 GHz has been developed. *Methods and Results*: The efficacy of the system was assessed through simulation and experiment on brain tissue mimicking phantoms under different setup conditions, where temperature and conductivity changes were accurately detected. In order to validate the radiometer's capability to sense low power signals occurring spontaneously from regions in the human brain, the somatosensory cortices of one volunteer were measured under pain inducing psychophysiological conditions. The promising results from the initial in-vivo measurements prove the system's potential for more extensive investigative trials. *Conclusion and significance*: The significance of this study lies on the development of a compact and sensitive radiometer for totally passive monitoring of local brain activation as a potential complementary tool for contributing to the research effort for investigating brain functionality.

***Index Terms*—Microwave radiometry, real time monitoring, non-invasive passive measurement, measurement of local brain temperature and / or conductivity variations**

I. INTRODUCTION

MICROWAVE radiometry has been long used in microwave medical imaging as a passive and entirely harmless technique to measure distributions of in depth tissue temperature applied both in diagnosis and therapy [1]–[4]. The main operation principle of this technique is the measurement of the chaotic thermal electromagnetic radiation, emitted by any lossy media at temperatures above the absolute zero. Using radiometry techniques, information about internal temperature patterns that could be used as complementary information in diagnosis as well as monitoring temperature changes during therapeutic procedures such as hyperthermia, is obtained [4], [5].

In parallel, functional imaging in neuroscience has known significant progress and gained imminent research interest due mainly to the opening of new paths in investigating different aspects of brain functionality. In this scientific milieu, it has been suggested that microwave radiometry may also provide estimations of local changes in conductivity and/or temperature in excitable tissues due to local changes in blood flow and volume [6]–[8]. These measurements could be linked to local brain activation potentially adding knowledge to other insights of brain functionality provided by well standardized imaging techniques such as fMRI and PET. During the past years various experiments, both in phantoms as well as in human volunteers, verify the contribution of microwave radiometry in temperature distribution imaging [9]–[11], but also indicate that radiometric systems may be able to pick up brain activation potentially due also to conductivity changes [6], [12].

In general, brain imaging devices are both bulky and expensive; all of them are also active imaging tools. Based on the aforementioned and with the effort to develop a low cost and portable system that could complement to the existing techniques, and possibly contribute to brain mapping, a new prototype microwave radiometry monitoring device is herein introduced. The thermal type radiation, emitted by the human body can be measured, by placing around the biological body a number of receiving sensitive antennas, as shown in Fig. 1. The signals are then measured and driven to a sensitive microwave receiver, a radiometer operating at 1.5 (+/-0.05) GHz. At 1.5 GHz there is sufficient penetration of microwave radiation into the head tissue, while we can still achieve significant imaging resolution [13]. The use of multiple antennas around the

20 October 2018

E. Groumpas and N. Uzunoglu are with the National Technical University of Athens, Zografou, Greece. (e-mail: egroumpas@mail.ntua.gr).

M. Koutsoupidou was with National Technical University of Athens, Greece. She is now with the Department of Informatics, King's College London, Bush House campus, London, UK. (e-mail: maria.koutsoupidou@kcl.ac.uk).

Irene S. Karanasiou is with the Department of Mathematics and Engineering Science, Hellenic Military Academy, Vari, Athens, Greece. (e-mail: ikaran@esd.ece.ntua.gr).

Charalabos Papageorgiou is with the Department of Psychiatry, Eginition Hospital, University of Athens. (email: Chpapag@med.uoa.gr)

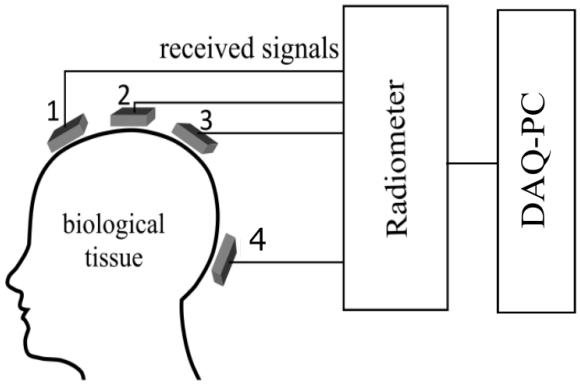

Fig. 1. System setup for sensing biological tissues with microwave radiometry.

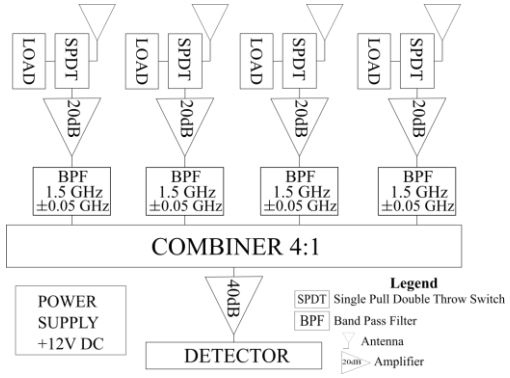

Fig. 2. Layout of the radiometer.

biological body enhances the in-depth detection ability as well as the sensitivity of the system. In this case four novel uniplanar elliptical antennas are placed around the head or phantom and the signal is fed to a custom-made radiometer. Numerous experiments in different setups have been carried out to investigate its functionality and monitoring attributes.

The paper is organized as follows. In Section II the components of the radiometer are described as well as the brain phantom that was used for the measurements. In Section III, a numerical analysis for calculating the field distribution generated by four antennas in a cubic phantom along with the field distribution generated by two and four antennas in a human head model is presented. It is followed by experiments with phantoms and respective results in Section IV. Results of the initial proof of concept experiments with a human volunteer are reported in Section V. In Section VI the experimental outcome is discussed and the paper concludes with a short evaluation of the radiometric prototype presented herein.

II. Materials And Methods

A. Radiometer

The developed system is used to collect the naturally emitted energy of the brain tissue. The collected energy is driven to a radiometer with a capability of power sensing down to -100 dBm. A total power Dicke-switch receiver operating at 1.5 (+/- 0.05) GHz is the main core of the radiometer. The receiver has four input ports where the antennas are connected. The received signals are driven through four similar chains of amplifiers and filters to a combiner and fed to the detector. The layout of the

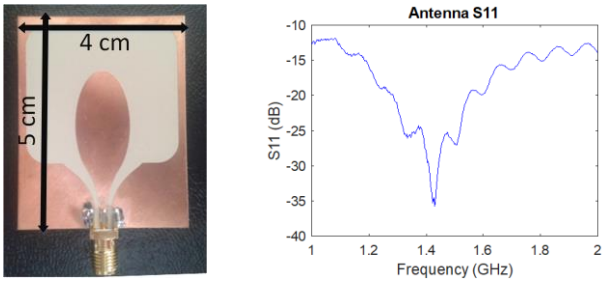

Fig. 3. (Left) The uniplanar elliptical antenna that was used in a 4-element array to sense the microwave signal radiated by the tissue. (Right) Measured reflection coefficient, S_{11}, of the uniplanar elliptical antenna when radiating into human tissue.

radiometer is shown in Fig. 2. The antenna is connected to a single pull double throw switch which is connected to a 50 Ohm load. The signal then passes through a 20 dB monolithic amplifier and a band pass filter (BPF) with 1.5 GHz center frequency and 0.1 GHz window. The power from each channel is combined and amplified in two stages by a total of 40 dB. Then a 65 dB power detector is used. A 12 V DC power supply is used with a regulator. Before the signal reaches the data acquisition card (DAQ), it passes through an amplifier and chip beads for noise removal. There is an on-off switch in each input channel; this way various combinations of antenna setups may be used either with one, some or all of the antennas connected to the radiometer. A 16 bit analog to digital acquisition card was used to collect the data. For the following experiments the sampling rate had been set at 10000 samples/s with averaging on every 1000 samples.

The power gathered by the radiometer's antennas is measured in terms of voltage at the output of the radiometric receiver based on the formula [9]:

$$I = \left(\frac{\omega_o^2 \mu_o k}{\pi}\right) \Delta\omega \iiint_V \Gamma_A(\vec{r}) T(\vec{r}) \sigma(\vec{r}) d\vec{r} \qquad (1)$$

where I is the computed average of the radiometer's output voltage, k is the Boltzman's constant, ω_0 is the centre frequency of the bandwidth of the observed microwave spectrum, μ_0 is the free space magnetic permeability, $\Delta\omega$ is the equivalent bandwidth, V is the volume of the focusing area, $T(\vec{r})$ is the temperature spatial distribution within the medium of interest, $\sigma(\vec{r})$ is the spatial distribution within the medium of interest for the electric conductivity, and $\Gamma_A(\vec{r})$ is the Kernel function related to the observed medium Green's function, taking into account the electromagnetic properties of the receiving antenna.

B. Antennas

The near field radiometric system comprises a 4-element array of uniplanar elliptical antennas (Fig.1). The reflection coefficient (S_{11}) of the selected antennas was measured -26 dB at 1.5 GHz band, when they lie on a human tissue, i.e. skin (Fig.3). The antennas exhibit a main lobe with gain of 3.1 dB and half-power beamwidth of 85 degrees according to simulation at 1.5 GHz. Additionally, previous studies have shown that an array of four antennas is capable to sense brain areas achieving a detection depth of more that 3 cm at 1.5 GHz [14], [15].

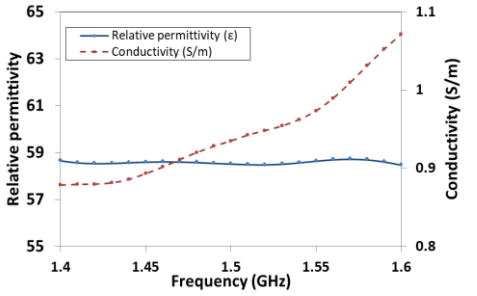

Fig. 4. Relative permittivity and conductivity of brain phantom measured in the 1.4-1.6 GHz range with open-ended coaxial cable method.

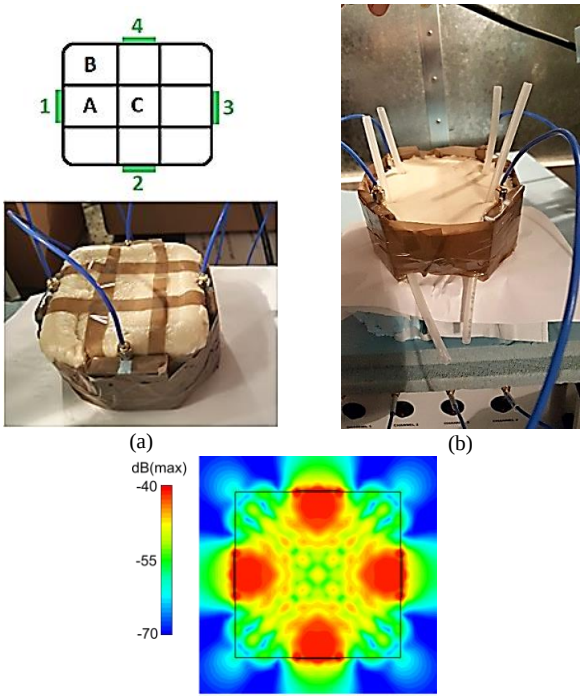

(a) (b)

(c)

Fig. 5. (a) Experimental setup for spatial sensitivity measurements: four antennas were placed around the cubic phantom, while it was divided into 9 cells for the thermal/conductivity source to be placed. Cell A: the middle sections of each side face of the phantom. Cell B: the corners of the phantom. Cell C: the center of the phantom. (b) Four straws placed 1cm from each antenna inside a second phantom were used to model blood flow. (c) Simulation results for the E-field distribution inside the cubic phantom at 1.5 GHz in a logarithmic scale.

C. Brain phantoms

To test the system's capability to sense localized temperature and conductivity changes, two brain phantoms were fabricated using water (64%), flour (33%) and gelatin (3%) [16]. The dielectric properties of the phantoms were measured with an open-end coaxial probe by SPEAG (DAK-12, SPEAG) and the results are presented in Fig. 4. At 1.5 GHz relative permittivity and conductivity are ε_r = 58. 5 and σ = 0.93 S/m. The first phantom was of cubic shape (10 cm x 10 cm x 7 cm) and it was used to test the spatial sensitivity of the system (Fig. 5 (a)). The second phantom was of hemispherical shape and combined with small straws, it was used in experimental setups mimicking local changes in blood flow (Fig. 5 (b)).

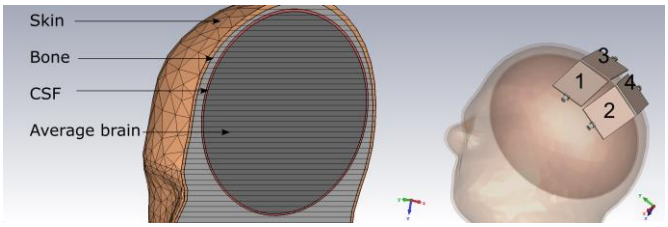

(a)

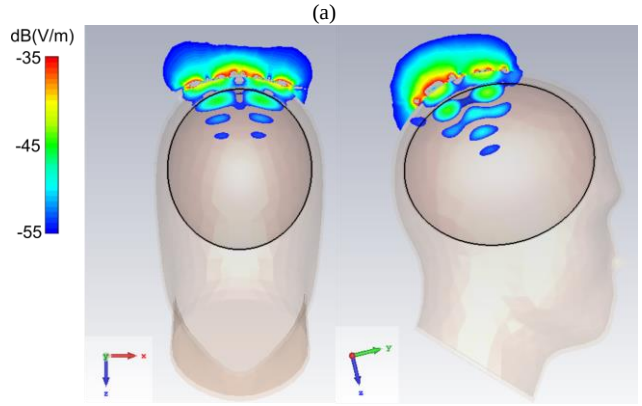

(b)

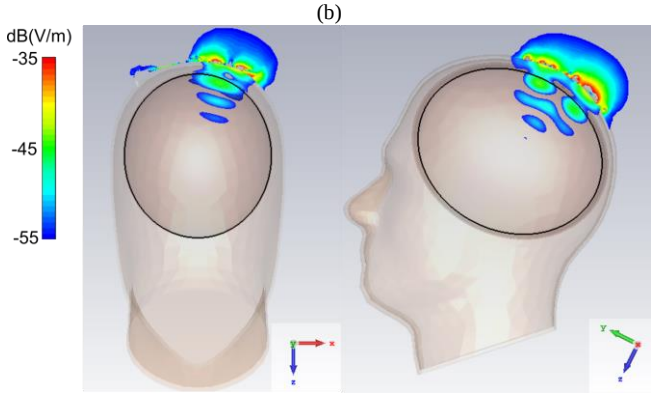

(c)

Fig. 6. (a) Simulation setup of four elliptical antennas radiating into a head model that comprises three layers with skin, bone and CSF and an ellipsoid internal volume with brain dielectric properties. (b) Simulation results for the E-field distribution inside the head model at the xz- and yz- plane at 1.5 GHz in a logarithmic scale. (c) Simulation results for the E-field distribution inside the head model at the xz- and yz- plane at 1.5 GHz in a logarithmic scale for 2 radiating antennas for the right hemisphere.

III. Numerical Analysis

The cubic phantom with four elliptical antennas placed on each vertical side of the phantom were modelled with CST Microwave Studio. Since microwave radiometry is a passive modality, the antennas operate as receivers. However, in order to reduce the computational cost, the reciprocal electromagnetic problem was solved according to the reciprocity theorem. Therefore, the electromagnetic field inside the phantom due to the excitation generated by the antennas was calculated at 1.5 GHz. The simulation results feature the electric field distribution inside the phantom for evaluating the field strength at different distances from the antennas (Fig. 5(c)). In a 2 cm x 2 cm area in front of each antenna the field is strongest, while it is reduced by 10-15 dB in the rest volume of the phantom.

A set-up of four elliptical antennas placed on top of a numerical head phantom was also modeled at 1.5 GHz. The head phantom comprised four layers whose dielectric properties

mimic that of skin (ε_r=44.4, σ =1.09 S/m), cancellous bone (ε_r=19.8, σ =0.45 S/m), cerebrospinal fluid (CSF) (ε_r=67.6, σ =2.72 S/m) and average brain (ε_r=45, σ =0.9 S/m) (Fig. 6(a)). The thicknesses of the three external layers were 8 mm (skin), 10 mm (bone) and 5 mm (CSF). Antennas 1 and 2 were placed to illuminate the left brain hemisphere, while antennas 3 and 4 were placed above the right hemisphere.

The electromagnetic field inside the head model due to the excitation generated by four antennas and two antennas was calculated at 1.5 GHz. The simulation results for the electric field distribution in the model by four and two antennas are shown in Fig. 6(b) and (c), respectively. The results are presented in a logarithmic scale with field strength below -60 dB clamped. Each antenna pair over the same hemisphere illuminates an area of 4 cm x 6 cm on the surface of the head. Additionally, this setup allows the creation of two focal points of small volume inside each brain hemisphere.

IV. Experiments On Brain Phantoms

The radiometer's capability to sense power levels down to -100 dBm renders it sensitive to external interference; hence all measurements were carried out in a Faraday chamber. The radiometer was placed inside the chamber along with the 4 antennas and the phantoms. The computer controlling the data acquisition process was placed outside the Faraday cage and was connected to the radiometer via Bayonet Neill–Concelman (BNC) connector interface through the cage's metallic wall.

A. Spatial sensitivity measurements

Four antennas were placed on the four side faces of the cubic phantom. The antennas topology on the phantom is shown in Fig. 5(a). The phantom was divided into nine equal cells. Cells A (x4) were the middle sections of each side face of the phantom and the closest to the antennas (Fig. 5.a): their center was distanced 2.5 cm from the respective antenna. Cells B (x4) were the corners of the phantom. Cell C (x1) is the middle section and its center is equally spaced from all antennas (5 cm). A 5 ml syringe was used to place the thermal or electrical conductive source into the phantom at the centers of these cells in order to test the spatial sensitivity of the radiometric system. All antennas were turned on during all experiments presented herein.

B. Flow measurements

Brain activation is often related to changes in local blood volume i.e. more blood crossing the vessels of the activated area. The changes in the volume of the vessels are translated to conductivity changes that passive microwave radiometry may be capable to monitor [9]. In order to simulate blood flow, the hemispherical brain phantom was pierced throughout with four narrow straws (2 mm inner radius) at 1 cm distance from each antenna (Fig. 5.b). A syringe was used to inject 5 ml of saline solution (0.5 M NaCl aqueous solution) inside the straw, while a glass underneath was used to collect the liquid. The syringe's tip was smoothly placed on one end of the straw and then the solution was injected through the phantom. The process was repeated four times in front of each antenna. During the first two trials, the syringe was placed at the tip and immediately the syringe was slowly and steadily pressed for 3 seconds in order to release the solution, causing a radiometer response over 7 seconds. The third time, the syringe was placed at the tip and after 5 seconds the solution was injected into the phantom almost instantaneously (1 second). Finally, for the last trial, after the smooth placement of the syringe, we waited for 20 seconds and then the solution was injected slowly (3 seconds) through the phantom. The water and the phantom were at room temperature during the whole duration of the experiment.

C. Conductivity sensitivity measurements

Four antennas were placed on the four side faces of the cubic phantom. The antennas topology on the phantom is shown in Fig. 5(a). A 20 ml syringe with normal saline (0.154 M) was placed 4 cm away from antenna 1. During the experiments, a blocked straw containing different concentrations of saline solutions was placed inside the syringe. In this experiment the focus was on detecting areas of higher conductivity (solution inside straw) inside a medium with constant conductivity (syringe with normal saline solution). Five different cases were examined. Initially, an empty straw (air), blocked at the bottom, was inserted in the syringe. Then, the straw was filled with normal saline solution (0.154 M). In that case the syringe (background) and the straw (target) were filled with solutions of the same salinity. For the following three cases, the straw was filled with saline solutions of 0.1617 M, 0.1771 M and 0.231 M, which correspond to a 5%, 15% and 50% NaCl concentration increase compared to normal saline. The experiment was repeated five times for each case.

D. Experimental results

The aim of the experiments described in Section IV was to examine the sensitivity of the proposed radiometric system to temperature and conductivity changes. Fig. 7.a shows the experimental results of the local temperature changes in cells C, B and A. The background noise generated a voltage output of 1.3430 V on average with standard deviation of $3x10^{-5}$ V. The thermal source, water at 40 ◦C, was detected with clear voltage spikes of 0.1 mV to 0.6 mV from the baseline. The presence of the thermal source at cells B and C resulted in increases of approximately 0.2 mV and 0.1 mV, respectively. The highest voltage increase, 0.6 mV, was observed when the thermal source was placed in cell A, in front of which antenna #1 had been positioned. Similar results were recorded for antennas #2, #3 and #4.

The results for the detection of conductivity changes are shown in Fig. 7.b. The background noise generated a baseline radiometric signal of 1.3430 V with standard deviation $3x10^{-5}$ V, while the saline solution was detected with clear increases of approximately 0.2 mV to 0.8 mV. At cell C the saline solution was detected with almost a 0.2 mV increase, while at cell B the increase was 0.25 mV. Similarly to temperature measurements, when the solution was placed close to the antenna (cell A) an increase of 0.8 mV was detected.

It is important to highlight that although in cell C the thermal

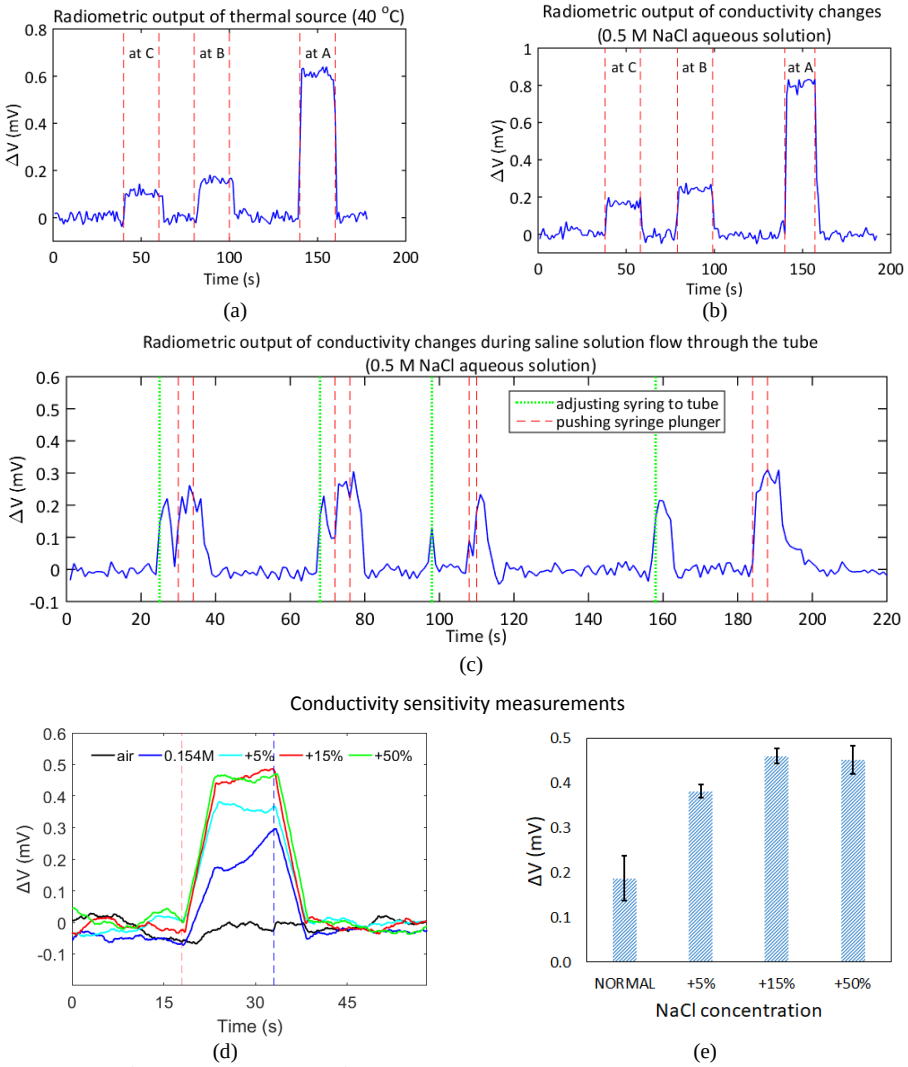

Fig. 7. (a) Radiometric voltage output of the experimental setup for local temperature changes when the small container was inserted into the cubic phantom sequentially at cells C, B and A around antenna #1. (b) Radiometric voltage output of the experimental setup for local conductivity changes when the saline solution inside the small container was inserted into the cubic phantom sequentially at cells C, B and A in proximity to antenna #1. (c) Radiometric voltage output of the experimental setup for local conductivity changes when saline solution was inserted into the straw in front of antenna #1. (d) Radiometric output when a blocked straw with air (black line), normal saline (blue) and saline solutions with 5% (cyan), 10% (red) and 50% (green) extra NaCl than the normal saline is inserted in a larger syringe filled with normal saline that lies inside the cubic brain phantom. The red dotted line approximates the insertion line and the blue dotted line the extraction time. (e) Average radiometric increase and respective error from 5 measurements of the conductivity sensitivity experiment using solutions of increasing salinity.

and conductivity source has maximum distance (5 cm) from all antennas, changes were clearly sensed by the radiometer with an output voltage increase that is comparable to cell B, which is distanced ~ 3.5 cm from the adjacent antennas. This is explained by the fact that when inside cell C the sources were sensed by all four antennas, while in cell B they were sensed by two antennas.

The flow experiments provided the results depicted in Fig. 7(c). The background noise generated a voltage output of 1.3470 V on average with 2×10^{-5} V standard deviation. The time slots of placing the syringe on the straw tip and pushing the plunger were recorded and depicted in Fig. 7(c). The vertical green and red dashed lines show when the vocal command to place the syringe on the tube was given and the approximate duration that the syringe plunger is being pushed. When the syringe was adjusted to the tip of the straw, a voltage fluctuation was detected. It is evident that the change is gradually reduced as soon as the setup is stable again. Then, the syringe is slowly pressed in order to create a constant flow or a burst of the saline solution through the phantom. The steady flow of the saline solution caused 0.3 mV increase with the anticipated steep curve. During the burst (third repetition), the output voltage increase related to the fast flow was 0.2 mV.

The results from the conductivity sensitivity measurements are depicted in Fig. 7(d) and (e). Fig. 7(d) shows voltage changes caused by the insertion of the blocked straw filled with air, normal saline (0.154 M) and solutions of increased salinity in a syringe with normal saline. The insertion of the empty blocked straw (air) does not present any significant fluctuation. The blue line (0.154 M) depicts the radiometer's output when the straw containing normal saline solution is inserted. The same holds for the rest saline solutions of 0.1617 M (cyan line),

0.1771 M (red line) and 0.231 M (green line), which correspond to a 5%, 15% and 50% increase in the NaCl concentration of the syringe content. It is obvious that the insertion of higher concentration saline solution in the syringe containing normal saline (0.154 M) causes an increased radiometric voltage output, as expected from Equation (1). Baseline during conductivity sensitivity measurements was at 1.3505 V with $3.2x10^{-5}$ V standard deviation. The average radiometric increase along with the respective error from five measurements for each saline solution concentration are illustrated in Fig. 7(e). The radiometric voltage output does not increase linearly with the salinity concentration.

V. INITIAL HUMAN EXPERIMENTS

In an attempt to test the functionality of the radiometer, initial experiments involving the participation of a human volunteer were carried out. The participant provided written informed consent and all experimental procedures involving the human volunteer were conducted in accordance with the declaration of Helsinki. It is known that brain responds to stimuli (i.e. temperature changes and pain), which activate certain regions of the brain cortex through increased regional cerebral blood flow (rCBF) [17]. One volunteer has been subjected to a brain stimulus test, the well-known Cold Pressor Test [18], [19] multiple times by immersing their contralateral and ipsilateral hand into cold and room temperature water. The antennas were attached on the internal surface of a helmet placed on top of the head (Fig.8). Only two adjacent antennas on the same hemisphere of the head were operating during each experimental procedure. According to simulation results in Section III, the antennas were sensing a projected on the head surface area of approximately 4 cm x 6 cm for each hemisphere. This area includes the primary somatosensory cortex that is responsible to process pain stimuli in brain among other functions [20]. The procedure was carried out on one subject for 4 times over a period of three months. The aim of this experiment is to show recurrence of the results and thus the feasibility of the system in vivo. The results of these experiments are not used to extract patterns or draw conclusions regarding the behavior of the brain or determine the relationship between stimuli and system's output. In future studies, with more human data enabling statistical analyses, such conclusions will be possible. These experiments aim to prove that the system's output voltage changes are caused by the experimental procedure, i.e. the Cold Pressor Test, and they are not generated randomly or by another physiological stimulus.

The experimental procedure is similar to the one presented in [9] and is as follows. Two antennas were connected and collecting data from one side of the head, i.e the right hemisphere. The subject was in a sitting position near the radiometer inside the Faraday chamber avoiding any movement. The same procedure was followed for the left hemisphere. The hand movement was performed by another person, in order to avoid as much as possible unnecessary movement by the subject during the test. Additionally, by asking the subject to have their hands loose and free to be moved, we tried to ensure no significant activity in the primary motor cortex that is adjoining the primary somatosensory cortex and could be sensed by the antenna array [18], [19], [21].

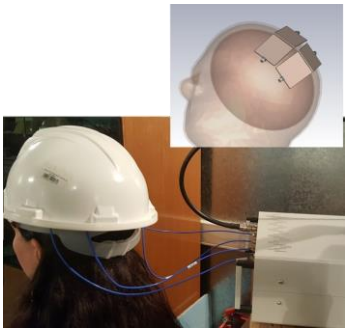

Fig. 8. Antenna array position on head and set-up for measuring brain activation in primary somatosensory cortex.

All actions during the measurements had one minute duration and were followed by one minute resting period. Two sets of experiments were carried out with the antennas being placed on only one side of the head, left or right for each experiment in order to view the responses of the left and right hemisphere, respectively. Four measurements have been taken for each experimental set. At first, the subject remained at resting state. Then, the contralateral and ipsilateral hand was immersed in room temperature water (28 ^{o}C) with resting periods in between. Following, the contralateral and ipsilateral hand was immersed into ice cold water. The experiment duration was 9 minutes with the subject being immobile. The procedure phases are shown in Table 1.

The average results of the four experimental procedures, which were conducted over a three month period, are displayed in Fig. 9. The vertical red dotted lines indicate the approximate time of hand immersion and removal action. It should be noted that the lines serve as an indication of the time the command is delivered and there might be a couple seconds variation between the command and the actual completion of the action. The blue lines in Fig. 9(a) and 9(b) show the average voltage change from baseline of four experiments measured with the radiometer when the antenna array was attached to the subject's right and left hemisphere during the Cold Pressor test, respectively. The black lines demonstrate the average voltage change of four experiments with the subject being at a resting state (without undergoing the Cold Pressor test or another physiological stimulus). A moving average filter with a window of 50 samples was applied to the collected data in post processing. Figures 9(a) and 9(b) elucidate the good repeatability of the measurements for each hemisphere. The output variations of each phase are distinct and consistent. The peak voltage changes have been measured and are presented in Table II. It can be deducted that radiometric output changes for the contralateral hand are greater in icy water than regular water for both hemispheres. The opposite holds for the ipsilateral fluctuations. Also, the fluctuation of the contralateral cold is greater than the ipsilateral cold. In previous work [9] it has been observed that the brain hemisphere controlling the dominant hand presents smaller fluctuations to the stimuli due to habituation. The obtained results are similar to the ones obtained in [9] and may suggest that the increased activities observed during pain stimulation reflect physiological differences in cortex activity mainly attributed to local changes of temperature and/or conductivity. These changes seem to be

linked to changes in cerebral blood flow and volume [9]. The changes to the radiometer's output may not be attributed to ionic releases or synaptic activity [9].

The distinction between the time intervals of the hand being inside and outside the water is evident. The most significant cause of noise is movement of the head that displaces the cables and the antennas may lose contact with the head surface.

Table I
Experimental Procedure

Time (s)	Graph Notation	Description
0-55	A1	Air, resting state 1
55-115	CR1	Contralateral hand immersed in room temperature water
115-175	A2	Air, resting state 2
175-235	IR1	Ipsilateral hand immersed in room temperature water
235-295	A3	Air, resting state 3
295-355	CC1	Contralateral hand immersed in cold water
355-415	A4	Air, resting state 4
415-475	IC1	Ipsilateral hand immersed in cold water
475-535	A5	Air, resting state 5

Table II
Peak Voltage

	Right (μV)	Left (μV)
CR	270	47
IR	-317	-71
CC	364	70
IC	-196	-43

VI. Discussion

Microwave radiometry could offer an entirely passive modality for sensing temperature and/or conductivity changes that are possibly related to specific brain functions and activation cortex regions. Currently, brain radiometry is mostly researched as deep-tissue thermometry for accurately and non-invasively monitoring brain temperature in infants [22] or during medical procedures, such as surgical operation and hyperthermia treatment [23]. Previous work of our group also involves the development of a system for focused microwave radiometry with enhanced sensitivity and spatial resolution [9], [24], where the patient needs to lie on a table with his head inside a body-size ellipsoidal cavity.

Following steps towards a portable radiometric system for a totally passive investigation of human brain functionality would involve the development of a more ergonomic antenna positioning system on the head surface setup that will minimize movement related noise. Also, ways to reduce EMI noise, such as shielding the antennas or a shielding cap, in order to perform experiments outside the Faraday chamber will be studied. Such a set-up would allow the clinical use of the device for large scale trials. However, considering that radiometric sensing is very sensitive to noise from external electromagnetic sources, it is preferable to measure subjects in a Faraday chamber at this stage of the system's development. Various combinations of

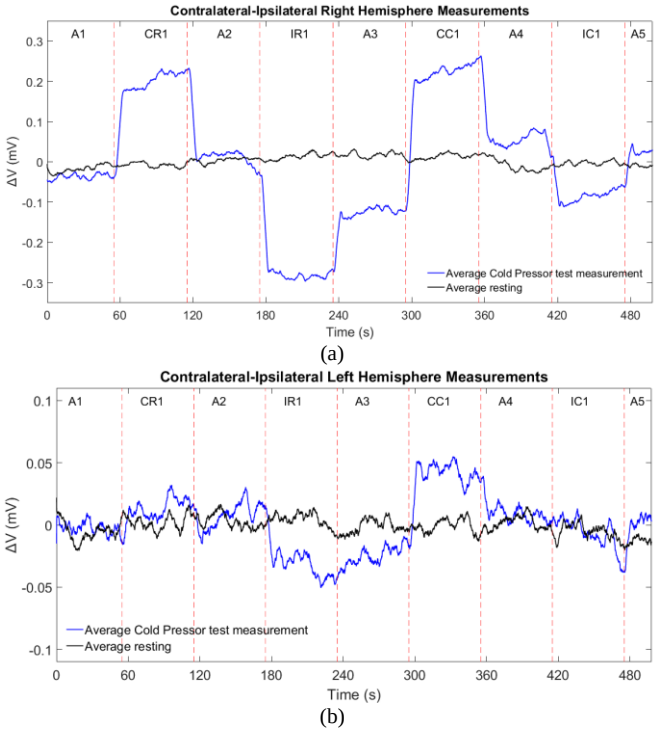

Fig. 9. (a) Average voltage change from baseline of four experiments measured with the radiometer when the antenna array was attached to the subject's right hemisphere during the Cold Pressor test (blue line) and at resting state (black line) (b) when the antenna array was attached to the subject's left hemisphere during the Cold Pressor test (blue line) and at resting state (black line).

number of antennas used and respective placement on the head surface will be also carried out. By activating less antennas, a smaller and more specific area of brain is sensed although the radiometric output change is more limited. For this study, using the simulation results as a guide, the antennas were placed slightly tilted on top of the head for creating a focal point at each brain hemisphere. Types of more directive antenna designs will be also tested. Concluding, however, initial results show that near field microwave radiometry could be a promising modality for investigating brain functionality.

VII. Conclusion

Herein, we propose a microwave system for near field brain radiometry that offers a more compact approach for bedside clinical usage compared to previously proposed systems. The electromagnetic profile created by four antennas in a numerical head phantom had been calculated in order to choose the appropriate set-up for in-vivo measurements. The experimental results presented in Section IV prove that the system can sense local temperature or conductivity changes at a distance up to 5 cm in a brain phantom. In a set-up that resembles more closely to local changes of blood volume, we have presented the system's ability to sense small volumes and fast changes of conductivity. Finally, the system was also used in proof-of-concept in vivo measurements where the brain cortex region associated with pain processing was activated during controlled human experiments. The primary somatosensory cortex of one volunteer was monitored while experiencing a well standardized stress test multiple times. The experiments aimed

to validate the system's functionality during in vivo measurements and its ability to sense low power signals from the human cortex. These signals are possibly related to local changes in blood concentrations in the activated regions that eventually result to temperature and/or conductivity changes.

REFERENCES

[1] Y. Birkelund et al., "Vesicouretal reflux in children: A phantom study of microwave heating and radiometric thermometry of pediatric bladder," *IEEE Transactions on Bio-Medical Engineering*, vol. 58, no. 11, pp. 3269–3278, Nov. 2011.

[2] P. R. Stauffer et al., "Stable Microwave Radiometry System for Long Term Monitoring of Deep Tissue Temperature," *Proceedings of SPIE*, vol. 8584, p. 10.1117/12.2003976, Feb. 2013.

[3] K. Toutouzas et al., "First In Vivo Application of Microwave Radiometry in Human Carotids: A New Noninvasive Method for Detection of Local Inflammatory Activation," *Journal of the American College of Cardiology*, vol. 59, no. 18, pp. 1645–1653, May 2012.

[4] K. T. Karathanasis et al., "Experimental Study of a Hybrid Microwave Radiometry—Hyperthermia Apparatus With the Use of an Anatomical Head Phantom," *IEEE Transactions on Information Technology in Biomedicine*, vol. 16, no. 2, pp. 241–247, Mar. 2012.

[5] S. Jacobsen and P. R. Stauffer, "Can we settle with single-band radiometric temperature monitoring during hyperthermia treatment of chestwall recurrence of breast cancer using a dual-mode transceiving applicator?," *Physics in Medicine & Biology*, vol. 52, no. 4, p. 911, 2007.

[6] I. S. Karanasiou and N. K. Uzunoglu, "Experimental study of 3D contactless conductivity detection using microwave radiometry: a possible method for investigation of brain conductivity fluctuations," in *The 26th Annual International Conference of the IEEE Engineering in Medicine and Biology Society*, 2004, vol. 1, pp. 2303–2306.

[7] M. R. Tofighi and C. T. Huynh, "A microwave system for blood perfusion measurements of tissue; a preliminary study," in *2013 IEEE Topical Conference on Biomedical Wireless Technologies, Networks, and Sensing Systems*, 2013, pp. 49–51.

[8] K. Toutouzas et al., "A new non-invasive method for detection of local inflammation in atherosclerotic plaques: Experimental application of microwave radiometry," *Atherosclerosis*, vol. 215, no. 1, pp. 82–89.

[9] I. S. Karanasiou et al., "Towards functional noninvasive imaging of excitable tissues inside the human body using focused microwave radiometry," *IEEE Transactions on Microwave Theory and Techniques*, vol. 52, no. 8, pp. 1898–1908, Aug. 2004.

[10] P. F. Maccarini et al., "A novel compact microwave radiometric sensor to noninvasively track deep tissue thermal profiles," in *2015 European Microwave Conference (EuMC)*, 2015, pp. 690–693.

[11] P. Momenroodaki et al., "Noninvasive Internal Body Temperature Tracking With Near-Field Microwave Radiometry," *IEEE Transactions on Microwave Theory and Techniques*, vol. PP, no. 99, pp. 1–11, 2017.

[12] I. S. Karanasiou and N. K. Uzunoglu, "Single-frequency and multiband microwave radiometry for feasible brain conductivity variation imaging during reactions to external stimuli," *Nuclear Instruments and Methods in Physics Research Section A: Accelerators, Spectrometers, Detectors and Associated Equipment*, vol. 569, no. 2, pp. 581–586, Dec. 2006.

[13] M. Bjelogrlic et al., "Experimental verification of optimal frequency range for microwave head imaging," in *2017 International Conference on Electromagnetics in Advanced Applications (ICEAA)*, 2017, pp. 1008–1011.

[14] E. Groumpas et al., "Sensing local temperature and conductivity changes in a brain phantom using near-field microwave radiometry," in *2017 International Workshop on Antenna Technology: Small Antennas, Innovative Structures, and Applications (iWAT)*, 2017, pp. 293–295.

[15] M. Koutsoupidou et al., "Evaluation of a tumor detection microwave system with a realistic breast phantom," *Microwave and Optical Technology Letters*, vol. 59, no. 1, pp. 6–10, 2017.

[16] B. J. Mohammed and A. M. Abbosh, "Realistic head phantom to test microwave systems for brain imaging," *Microwave and Optical Technology Letters*, vol. 56, no. 4, pp. 979–982, 2014.

[17] R. Peyron et al., "Functional imaging of brain responses to pain. A review and meta-analysis (2000)," *Neurophysiologie Clinique/Clinical Neurophysiology*, vol. 30, no. 5, pp. 263–288, Oct. 2000.

[18] K. L. Casey, "Forebrain mechanisms of nociception and pain: Analysis through imaging," *Proceedings of the National Academy of Sciences of the United States of America*, vol. 96, no. 14, pp. 7668–7674, Jul. 1999.

[19] P. Petrovic et al., "A Regression Analysis Study of the Primary Somatosensory Cortex during Pain," *NeuroImage*, vol. 16, no. 4, pp. 1142–1150, Aug. 2002.

[20] K. D. Bornhövd et al., "Painful stimuli evoke different stimulus-response functions in the amygdala, prefrontal, insula and somatosensory cortex: a single-trial fMRI study," *Brain : a journal of neurology*, vol. 125 Pt 6, pp. 1326–36, 2002.

[21] S. La Cesa et al., "fMRI pain activation in the periaqueductal gray in healthy volunteers during the cold pressor test," *Magnetic Resonance Imaging*, vol. 32, no. 3, pp. 236–240.

[22] J. W. Hand et al., "Monitoring of deep brain temperature in infants using multi-frequency microwave radiometry and thermal modelling," *Physics in Medicine & Biology*, vol. 46, no. 7, p. 1885, 2001.

[23] P. R. Stauffer et al., "Non-Invasive Measurement of Brain Temperature with Microwave Radiometry: Demonstration in a Head Phantom and Clinical Case," *The neuroradiology journal*, vol. 27, no. 1, pp. 3–12, Feb. 2014.

[24] M. Koutsoupidou et al., "The effect of using a dielectric matching medium in focused microwave radiometry: an anatomically detailed head model study," *Med Biol Eng Comput*, pp. 1–8, Oct. 2017.